

Chapter 6

Tunable Exchange Bias Effects

Ch. Binek

Abstract Extrinsic control mechanisms of the interface magnetization in exchange bias heterostructures are reviewed. Experimental progress in the realization of adjustable exchange bias is discussed with special emphasis on electrically tunable exchange bias fields in magnetic thin film heterostructures. Current experimental attempts and concepts of electrically controlled exchange bias exploit magnetic bilayer structures where a ferromagnetic top electrode is in close proximity of magnetoelectric antiferromagnets, multiferroic pinning layers, or piezoelectric thin films. Various experimental approaches are introduced and the potential use of electrically controlled exchange bias in spintronic applications is briefly outlined. In addition, isothermal magnetic field tuning of exchange bias fields and extrinsically tailored exchange bias training effects are reported. The latter have been studied in a variety of systems ranging from conventional antiferromagnetic/ferromagnetic bilayers and core-shell nanoparticles to all ferromagnetic heterostructures where soft and hard ferromagnetic thin films are exchange coupled across a non-magnetic spacer. Such ferromagnetic bilayers show remarkable analogies to conventional exchange bias systems. At the same time they have the experimental advantage to provide direct access to the magnetic state of the pinning layer by simple magnetometry. A large number of exchange-coupled magnetic systems with qualitative differences in materials composition and coupling share a common physical principle that gives rise to training or aging phenomena in a unifying framework. Deviations from the equilibrium spin configuration of the pinning layer generate a force that drives the system back toward equilibrium. The initial nonequilibrium states can be tuned by temperature and applied set fields providing control over various characteristics of the training effect ranging from enhancement to complete quenching.

Ch. Binek (✉)

Department of Physics and Astronomy and the Nebraska Center for Materials and Nanoscience,
University of Nebraska, Lincoln, NE 68588, USA
e-mail: cbinek2@unlnotes.unl.edu

6.1 Introduction

Proximity effects in general and those of magnetic materials in particular are cornerstones of modern condensed matter physics. The investigation of exchange-coupled magnetic thin films has enormous technological importance particularly for applications which utilize spin-dependent transport across magnetic interfaces [1–4]. Exchange bias (EB) is a prototypical magnetic proximity phenomenon widely used in modern magnetic field sensors and read heads exploiting giant magnetoresistance (GMR) and tunnel magnetoresistance (TMR) effects. Scalability of read head sizes toward smaller devices is a prerequisite for the ongoing exponential growth of the areal storage density in magnetic hard disk drives. Remarkably, this exponential growth known as Moore’s law [5] shows an even increased rate since 1997 when GMR-based read heads with exchange-biased electrodes were first introduced in hard drive technology.

The basic physics of the EB phenomenon is best studied at the interface of exchange-coupled ferromagnetic (FM) and antiferromagnetic (AF) heterostructures [6–12]. In the proximity of an AF pinning layer a FM film can experience an exchange-induced unidirectional anisotropy. The latter reflects its presence most prominently by a shift of the FM hysteresis along the magnetic field axis and is quantified by the amount $\mu_0 H_{\text{EB}}$ of the shift. The EB effect is initialized when field cooling an AF/FM heterosystem to below the blocking temperature, T_B , where AF order establishes at least on mesoscopic scales [13].

Microscopically the EB phenomenon depends on a large number of system-specific details like structural and magnetic interface roughness and anisotropy to name just a few. Therefore, a large number of theories have been proposed competing to explain the origin of the EB effect. This chapter will not attempt to give an overview of the microscopic theories or even favor a particular microscopic mechanism over another one. The interested reader is referred to a number of excellent review articles with emphasis on experimental and theoretical aspects, respectively [8–11, 14].

Despite the ongoing controversy about “the origin” of EB many of the macroscopic observations are satisfactorily summarized in the phenomenological description which goes back to Meiklejohn and Bean. It has often been stated that the Meiklejohn–Bean (MB) expression is an invalid oversimplification which overestimates the expected EB field typically by more than an order of magnitude. This overestimation arises when bulk properties and ideal interface conditions are naively assumed. However, when using the MB expression in its appropriate phenomenological sense and the non-trivial relation between macroscopic and microscopic parameters is carefully considered, the MB approach remains a useful description with even quantitative predictive power. State-of-the-art molecular beam epitaxial growth of EB heterostructures allows the fabrication of nearly ideal interfaces with no or negligible roughness on mesoscopic lateral length scales. In fact, such ideal interface regions follow precisely the MB prediction of vanishing EB for compensated AF interfaces [15]. Similar results are known already for nearly a decade now from experiments using artificial AF superlattices as virtually ideal pinning systems

confirming the MB approach [16]. Therefore, it is meanwhile widely accepted that EB requires a net irreversible AF interface magnetization S_{AF} coupling via exchange with the FM interface magnetization S_{FM} [17]. It turns out to be the major challenge for microscopic theories to explain why S_{AF} can be surprisingly large for antiferromagnets with compensated AF surfaces and can be surprisingly low in systems with uncompensated surfaces. The MB description does not address these questions. It is therefore not a flaw of the MB approach when unrealistic values for S_{AF} for instance are used which consequently overestimate the EB fields. It is one of the major experimental and theoretical insights in recent years that only a fraction of the AF interface magnetization remains stationary during the FM magnetization reversal. It is this stationary or irreversible fraction S_{AF} of the AF interface magnetization that should be used in the MB expression to estimate realistic EB field values.

Another potential flaw of the MB approach originating from the assumption of uniform rotation of the ferromagnet seems also significantly overrated. Intrinsic properties which determine for instance the absolute values of the coercive fields and the magnetization reversal process are not necessarily relevant for the EB field, only their asymmetry with respect to the magnetic zero field determines the EB field. The latter is therefore insensitive on microscopic and micromagnetic details as long as they do not affect the irreversible interface magnetization.

When considering the exchange coupling of strength J between S_{AF} and the FM interface magnetization, S_{FM} , as phenomenological parameters the original MB approach describes in fact major features of the EB effect in a correct manner. In particular, the EB field, $\mu_0 H_{EB}$, quantifying the shift of the FM hysteresis loop along the magnetic field axis is in its simplest form expressed as

$$\mu_0 H_{EB} = -\frac{J S_{AF} S_{FM}}{M_{FM} t_{FM}}, \quad (6.1)$$

where M_{FM} is the saturation magnetization of the FM film and t_{FM} is its thickness. The latter inverse thickness dependence on the FM film has been confirmed in countless investigations and reflects the true interface nature of the effect. Experimentally this interface sensitivity implies that control over interface properties is crucial for systematic studies of the phenomenon.

Meiklejohn and Bean derived Eq. (6.1) from the Stoner–Wohlfarth type model where uniform rotation of FM magnetization is induced by a magnetic field applied along the easy AF and FM axes. In addition to the free Stoner–Wohlfarth ferromagnet, exchange coupling at the interface between the ferromagnet and a stationary AF pinning system of infinite anisotropy is the major ingredient of the simple MB model. Equation (6.1) is analytically derived from the MB energy expression. The most convenient and original MB approach contracts the Zeeman and the AF/FM coupling energy into an effective Zeeman term where the renormalized field is interpreted as the sum of the applied field and $\mu_0 H_{EB}$.

MB-type approaches have been studied for a variety of generalizations including finite anisotropy of the antiferromagnet, finite AF film thickness, and arbitrary orientation of the applied field with respect to the easy axes to name just a few [18].

In contrast to the usual analytic MB approach discussed elsewhere, Fig. 6.1 provides a graphical illustration associated with the evolution of the MB energy on variation of the magnetic field. Here, as an example, the applied magnetic field makes an angle of $\alpha = \pi/6$ with respect to the easy axis of the Stoner–Wohlfarth-type ferromagnet with uniaxial anisotropy of energy density K . The displayed hysteresis loop, M/M_s vs. h , represents the projection, $M = M_s \cos(\alpha - \beta_{\min}(h))$, of the uniformly rotating magnetization vector \underline{M} of magnitude M_s onto the direction of the reduced magnetic field $h = \mu_0 M_s t_{\text{FM}} H$. Rotation of \underline{M} takes place in accordance with the evolution of the angle $\beta_{\min} = \beta_{\min}(h)$. The latter follows a crossover from a global energy minimum into a local minimum on approaching the coercive fields h_{c1} and h_{c2} , respectively. In addition to the hysteretic M/M_s vs. h curve the evolution of the corresponding energy density

$$E/A = -h \cos(\alpha - \beta) + K \sin^2 \beta - J S_{\text{AF}} S_{\text{FM}} \cos \beta \quad (6.2)$$

is plotted with $K=0.5$, $J S_{\text{AF}} S_{\text{FM}} = 0.2$ (solid line) for selected fields $h = \pm 2$ (upper right and lower left insets), and for the switching fields $h = h_{c1}$ (upper left inset) and $h = h_{c2}$ (lower right inset) where M changes sign, respectively. It is the asymmetry of the switching fields with respect to $h=0$ which determines the EB field $h_{\text{EB}} = (h_{c1} + h_{c2})/2$. Full lines in the insets of Fig. 6.1 show the respective energy densities when exchange coupling between the ferromagnet and the AF pinning layer is included. The dashed curves show the corresponding energy densities of the same Stoner–Wohlfarth ferromagnet in the absence of coupling ($J = 0$). The comparison of these energy curves in particular at h_{c1} and h_{c2} illustrates the mechanism giving rise to the EB shift h_{EB} .

In the presence of the strong positive field $h=2$ the magnetization vector aligns virtually parallel to the magnetic field. Here, in a state close to positive saturation, the Zeeman energy controls the pronounced minimum in E/A vs. β where β measures the orientation of the magnetization with respect to the easy axis of the ferromagnet. The dominance of the Zeeman energy over the AF/FM coupling energy is reflected in the fact that the energy densities with (solid line) and without coupling (dashed line) virtually coincide. On lowering the magnetic field toward $h = h_{c1}$, antiparallel orientation of M with respect to the applied field becomes unstable. The instability is reflected by a saddle point in E/A vs. β . The dashed curve in the upper left diagram of Fig. 6.1 indicates that in the absence of interface coupling the instability and, hence, magnetization reversal set in at $h_{c1}(J = 0) = h_{c1} - h_{\text{EB}}$. Finally, negative saturation at $h = -2$ is virtually achieved, corresponding to a pronounced minimum in E/A vs. β and parallel alignment of the magnetization vector with the applied field. With increasing magnetic field again antiparallel alignment of M with respect to h becomes unstable in accordance with a saddle point in E/A vs. β at $h_{c2} = h_{c2}(J = 0) + h_{\text{EB}}$. This switching field is lowered by the amount $|h_{\text{EB}}|$ in comparison to the switching field of the unpinned Stoner–Wohlfarth ferromagnet

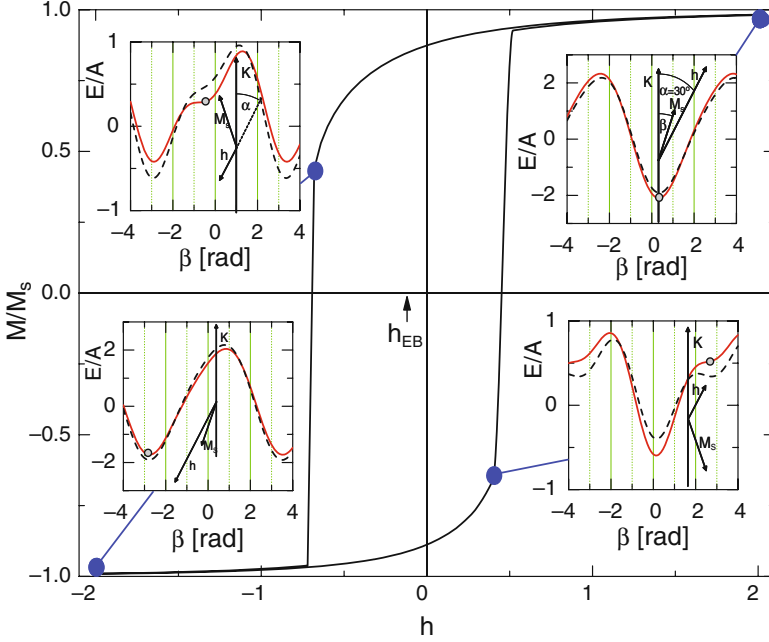


Fig. 6.1 Field dependence M/M_s vs. h of a uniaxial anisotropic Stoner–Wohlfarth ferromagnet exchange coupled to the stationary and field-independent interface magnetization of an adjacent pinning system. The coupling gives rise to the exchange bias effect shifting the loop along the field axis by the amount $|h_{EB}|$ indicated by an arrow. Insets show the energy densities E/A vs. β for $h = 2$ (upper right), $h = h_{c1}$ (upper left), $h = -2$ (lower left), and $h = h_{c2}$ (lower right) with (solid lines) and without (dashed lines) exchange coupling. Magnetization states of specific interest are marked by large dots on the M/M_s vs. h curve. The corresponding minima in E/A vs. β are indicated in the energy densities by small dots. Pictograms show the easy axis of the ferromagnet of anisotropy energy density K and the relative orientation of the magnetization and the magnetic field. The former rotates uniformly with constant magnitude M_s in contrast to h which is applied under a constant angle of $\alpha = \pi/6$ with respect to the easy axis

$[h_{c2}(J = 0)]$. The dashed E/A vs. β curve in the lower right inset of Fig. 6.1 shows still a clear local minimum when the actual system with coupling evolves already into the saddle point instability.

The shift of the FM hysteresis loop along the magnetic field axis is often accompanied by an EB-induced loop broadening [19, 20]. This effect is not included in the MB description. The understanding of the loop broadening makes it necessary to consider the role of the loosely coupled majority fraction of AF interface spins which do not affect the EB field. The magnetic moment of these loose spins is not irreversible but follows to some extent the magnetization reversal of the top ferromagnet giving rise to a drag effect which broadens the FM hysteresis. More quantitatively based on mean-field arguments it has been predicted that the FM coercivity is related to the AF interface susceptibility [21]. Loosely coupled spins

are in particular sensitive to either exchange or applied magnetic fields and, hence, increase the AF interface susceptibility and by that the FM coercivity. The coercivity enhancement accompanies the EB effect and is characteristically reduced when the blocking temperature T_B of vanishing EB is approached from $T < T_B$. While loosely coupled moments flip easier when their AF neighboring spins lost long-range order, nevertheless a drag effect on the adjacent FM film is still present above the blocking temperature and even above the Néel temperature, T_N , of the pinning layer allowing for persistence of loop broadening above T_N .

In addition to the EB loop shift and broadening, a gradual degradation of the EB field can take place when cycling the heterostructure through consecutive hysteresis loops [22–32]. This aging phenomenon is known as training effect. It is quantified by the $\mu_0 H_{EB}$ vs. n -dependence, where n labels the number of loops cycled after initializing the EB via field cooling. EB and its accompanying training effect have been observed in various magnetic systems [8, 33–39]. The MB expression does not directly address the phenomenon of EB training. However, Eq. (6.1) correlates the bias field with the AF interface magnetization S_{AF} . The latter can and typically does change during successively cycled hysteresis loops of the FM top layer such that $S_{AF} = S_{AF}(n)$ gives rise to an n -dependence in $\mu_0 H_{EB}$. This chapter dedicates a section on the recent progress in understanding aging phenomena in various exchange-coupled systems. Selected experiments evidence certain control over the aging effects through the initialization protocol that sets the magnetization state of the pinning system.

While many intrinsic details of the EB phenomenon are still a matter of scientific debate, extrinsic control of the EB has been added in recent years to the major research topics in this field. Among the various possible control mechanisms, electrically tuned EB appears most attractive for spintronic applications. Research on electrically controlled EB has been initiated by work on $\text{Cr}_2\text{O}_3/\text{CoPt}$ heterostructures stimulating at the same time a revived interest in magnetoelectric materials. The same motivation, namely control of magnetism via electric fields, created recently a tremendous renewed interest in multiferroic materials where multiple ferroic order parameters (magnetic, electric, and elastic) can be simultaneously present and sometimes significantly couple. Conjugate magnetic and electric fields can be used to manipulate the respective cross-coupled order parameter. Switching of FM order by an electric field for instance promises significant impact in the design of future spintronic devices. Note, however, that the magnetoelectric effect does not require multiferroics and multiferroics do not necessarily show appreciable magnetoelectric effects. Actually in most cases they do not [40]. Nevertheless, some of the multiferroic materials promise potential for spintronic applications in addition to their more general exciting physical properties. Most recently studied multiferroics can be classified into single-phase and two-phase systems. Single-phase multiferroics are predicted to be rare [41]; however, many perovskite-type oxides have been successfully exploited to control magnetic order to some extent by electrical means and vice versa.

Next, various attempts of electric and magnetic field control of EB-related phenomena are introduced. Some of them are based on multiferroics and most are not.

6.2 Electrically Tuned Exchange Bias

6.2.1 Electrically Tuned Exchange Bias with Magnetolectrics

Experiments on the perpendicular EB heterostructure $\text{Cr}_2\text{O}_3/\text{CoPt}$ pioneered the field of electrically tuned EB [42–46]. Here the magnetolectric Cr_2O_3 has a twofold role. It serves as an AF pinning layer allowing at the same time for electrical tuning of the AF interface magnetization. Exchange coupling of the latter with the FM interface magnetization of the perpendicular anisotropic CoPt gives rise to electrically tunable interface coupling energy and, hence, to electrically tunable EB fields. The AF Cr_2O_3 is a prototypical magnetolectric material. Its intrinsic magnetolectric effect sets in below the Néel temperature, $T_N = 307$ K, together with AF long-range order when spatial and time inversion symmetry are broken, respectively, but build a symmetry operation in combination. AF magnetolectrics do not depend on spontaneous ferroelectric polarization to achieve coupling between the magnetization and an electric field and are therefore complementary to the multiferroic materials discussed in Section 6.2.2.

In a magnetolectric material an applied electric field induces a net magnetic moment which can be used to electrically manipulate the magnetic states of adjacent exchange-coupled FM films. More specifically, the linear magnetolectric effect is characterized by a linear magnetic response M^i (electric response P^i) induced by the application of an electric field E_j (magnetic field H_j) such that $\mu_0 M^i = \alpha_{\text{me}}^{ij} E_j$ and $P^i = \alpha_{\text{em}}^{ij} H_j$, where $\alpha_{\text{em}}^{ij} = \alpha_{\text{me}}^{ji} = \alpha_{\text{em}}^{ji}$ are the tensors of magnetolectric susceptibility and its transpose counterpart while i, j label the vector and tensor components, respectively [47, 48]. The magnetolectric susceptibility tensor α_{me}^{ij} of Cr_2O_3 has diagonal structure with $\alpha_{\text{me}}^{11} = \alpha_{\text{me}}^{22} = \alpha_{\perp}$ and $\alpha_{\text{me}}^{33} = \alpha_{\parallel} \approx 4.13$ ps/m at its maximum value achieved close to $T = 263$ K. This magnetolectric susceptibility is small in comparison to some other magnetolectric materials [49]. However, the AF nature of Cr_2O_3 and its appreciably high T_N still make it a first choice candidate for an intrinsic magnetolectric material when applications at or close to room temperature are envisioned.

Figure 6.2 shows the schematics of a $\text{Cr}_2\text{O}_3/\text{CoPt}$ heterostructure for electrically tunable EB. Here the electric field orients along the (111) direction of Cr_2O_3 taking advantage of the parallel magnetolectric susceptibility. Note that EB requires a non-zero projection of S_{AF} on S_{FM} making a top ferromagnet with perpendicular anisotropy mandatory when α_{\parallel} is used.

The current status of the description of the microscopic origin of the magnetolectric effect in Cr_2O_3 has been summarized by Alexander and Shtrikman [50] and by Hornreich and Shtrikman [51]. Figure 6.2 shows a sketch of a section of the unit cell of Cr_2O_3 . It indicates the A (spin up) and B (spin down) sites of the Cr^{3+} ions along the threefold rotation axis. In the presence of a positive applied electric field, the Cr^{3+} ion on the A site moves toward the upper triangle of O^{2-} ions. The corresponding ion on the B site moves in the same direction along the symmetry axis toward the smaller triangle of O^{2-} ions. The latter triangle is shared among the two

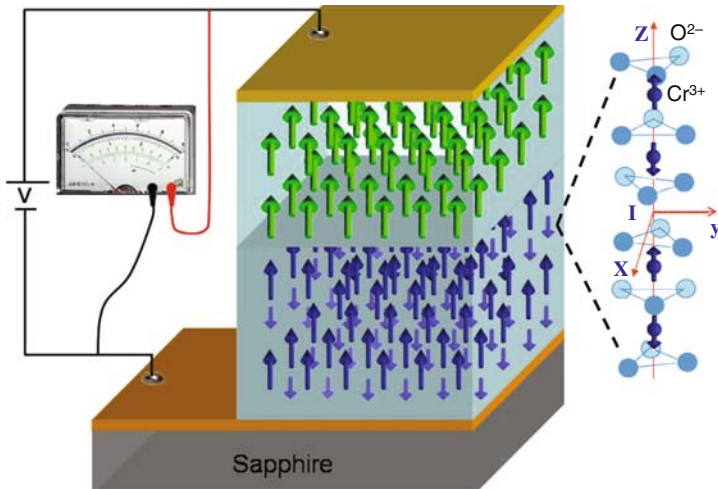


Fig. 6.2 Sketch of an electrically controlled EB heterosystem based on the magnetoelectric anti-ferromagnet Cr_2O_3 and a thin exchange-coupled CoPt multilayer. A voltage V applied across the *top* and *bottom* electrodes creates an electric field $E = V/d$ where d is the thickness of the insulating Cr_2O_3 film. The E field induced the magnetization $\Delta M \propto \alpha_{\parallel} E$ in Cr_2O_3 . It contributes to the interface magnetization S_{AF} and modifies the EB field. Arrows indicate the AF and FM spin structure in the Cr_2O_3 bottom and CoPt top layer, respectively. The right sketch depicts the crystal and spin structure of Cr_2O_3 . The spin orientations in the four sublattices are shown for one of the two 180° domains. The $S = 3/2$ spins of the Cr^{3+} ions are aligned along the threefold symmetry axis. O^{2-} ions form distorted octahedrons (distortion not shown) surrounding the Cr^{3+} ions. Electrically induced displacement of the latter into crystal fields of alternating higher and lower strength gives rise to the single ion contribution of the magnetoelectric effect (see text)

distorted octahedra of O^{2-} ions, which surround the Cr^{3+} ions on the A and B sites. The asymmetry in the change of the crystal fields experienced by A and B ions gives rise to the single-ion contributions of the magnetoelectric effect. In terms of a spin Hamiltonian, the single-ion contributions reflect the changes of the Landé g -tensor and the single-ion anisotropy, which differ for the spins at position A and B in the presence of an electric field. In addition, the asymmetric displacement of the ions gives rise to different modifications of the exchange interaction between Cr^{3+} ions. The resulting electric field-induced change of the exchange integrals is known as the two-ion contribution to the magnetoelectric effect.

Electric control of the EB field can be approached at least in two very distinct ways. An electric field can be applied simultaneously with a magnetic field in order to magnetoelectrically anneal the AF pinning layer. Magnetoelectric annealing is a well-known procedure to bring a magnetoelectric antiferromagnet into a single domain state by cooling the system from $T > T_N$ to below T_N in the presence of E and B fields. By energetically favoring one of the AF 180° domains over the other, the magnetic state of the AF interface magnetization is selected too and at least partially irreversibly frozen in. In an EB system using a magnetoelectric pinning layer the interface magnetic state can be magnetoelectrically selected. This type of

electric-controlled EB has been named magnetoelectric switching because it allows switching between positive and negative EB fields by controlling the sign of the product $E \cdot B$ [39]. This pronounced effect is highly interesting from a fundamental point of view. Spintronic applications, however, favor an electric control of the EB field at constant $T < T_N$ where ideally T_N is significantly above room temperature.

Recently, a reversible electrically induced shift of the magnetic hysteresis loops along the magnetic field axis has been achieved. The heterostructure follows the schema in Fig. 6.2 and is based for the first time on an all thin film $c\text{-Al}_2\text{O}_3/\text{Pt}5.7\text{nm}/\text{Cr}_2\text{O}_3$ 50 nm/ Pt 0.5 nm/ $[\text{Co}$ 0.3 nm/ Pt 1.5 nm] $_3/\text{Pt}$ 1.5 nm heterostructure.

Similar experiments have been performed earlier in $\text{Cr}_2\text{O}_3(111)/\text{CoPt}$ heterostructures using bulk Cr_2O_3 single crystals as AF pinning systems with magnetoelectric properties [40, 41]. Note, however, that millimeter thick single crystals require orders of magnitude higher voltages to achieve the electric fields that can be realized in nanometer thin films by a few millivolts. It is important to stress that the electrically controlled EB shown in Fig. 6.3 resembles a global effect. Here the tunable exchange anisotropy affects the entire FM top electrode and the EB field can be reversibly changed back and forth with the applied electric field. Competing EB systems based on multiferroic pinning layers show significantly larger isothermal EB tuning effect but are limited so far to local or irreversible control [52, 53]. A variety of spintronic applications based on electrically controlled exchange bias have been proposed. Those concepts of spintronic applications using electrically controlled EB have been pioneered by the authors in Refs. [42, 43]. Here spin-dependent transport

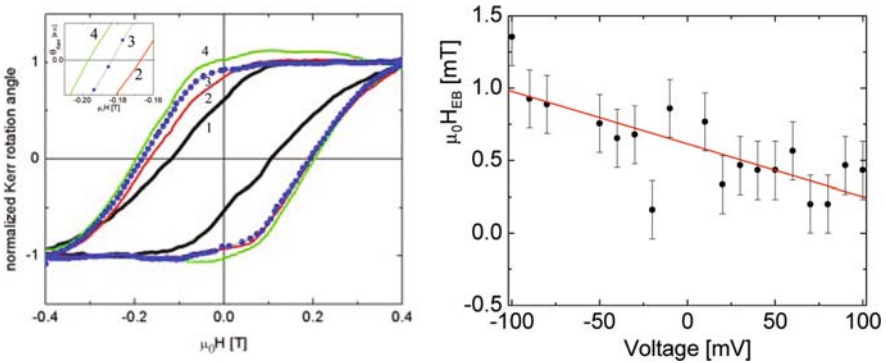


Fig. 6.3 The *left* frame shows normalized magnetic hysteresis loops of the all thin film $\text{Cr}_2\text{O}_3(111)/\text{CoPt}$ heterostructure measured by polar magneto-optical Kerr effect. Loop 1 is measured at $T=300$ K. Loops 2, 3, and 4 are measured after magnetoelectric annealing in $\mu_0 H = -0.4$ T and $V = -100$ mV from $T=300$ K to $T=250$ K $< T_N$. The isothermal loops have then been measured at $T=250$ K in the presence of applied axial voltages $V = -100$ mV (2), $+90$ mV (3), and $+100$ mV (4), respectively. The inset in the left frame provides a detailed look onto the electrically controlled change of the negative coercive fields of loops 2, 3, and 4. The right frame depicts the systematic results of the electric field control of the exchange bias field. The line is a linear best fit to the $\mu_0 H_{EB}$ vs. V data

devices with electrically controlled resistance states have been suggested. In general, magnetoelectrically induced interface magnetization provides control of the pinning in exchange-biased GMR- or TMR-type structures. In the GMR-type structures the active magnetoelectric material is used as a tunable pinning bottom layer offering new versatility for logic and memory devices based on a change of resistance due to a change of the magnetic configurations. In TMR-type structures the conventional passive tunneling barrier can be replaced by a magnetoelectrically active barrier material [42]. The electric field-induced magnetization of the latter allows switching magnetic states of exchange-coupled layers by pure electrical means. Following these suggestions numerous variations have been proposed [54]; often the magnetoelectric antiferromagnet has been replaced by a multiferroic component like BiFeO_3 [55–57].

6.2.2 Electrically Tuned Exchange Bias with Multiferroics

The above discussed attempts to achieve electrically tuned EB with the help of magnetoelectric antiferromagnets require further investigations and show clearly the need for an increase of the magnetoelectric response in order to accomplish appreciable electric tuning effects. In the case of magnetoelectric antiferromagnets significant efforts are made to further improve the structural and dielectric properties of Cr_2O_3 films allowing for higher applied electric fields and improved interface coupling [58].

Many research teams who currently focus on the use of multiferroic materials expect a qualitative progress from this class of materials. The latter show simultaneous presence of two or more ferroic order parameters like ferroelectric polarization and (anti)ferromagnetic order. This coexistence seems to make them obvious candidates for the quest of increased magnetoelectric response. The renewed excitement about multiferroics for spintronic applications is based on this hope. It is supported by a fundamental inequality which states that the square of the magnetoelectric susceptibility is limited by the product of the magnetic and the dielectric susceptibility [59]. Since multiferroics have spontaneous ferroelectric and ferromagnetic order the latter susceptibilities are high and their product limiting the magnetoelectric susceptibility α is high. However, to take advantage of this potential upper limit of α strong coupling between the ferroic order parameters is required. The coupling is, however, typically weak. Hence, the magnetoelectric susceptibility of most multiferroics is at room temperature or above disappointingly weak and it is not straightforward to exceed the magnetoelectric bulk susceptibility of, e.g., Cr_2O_3 which is of the order of 4 ps/m close to room temperature [60]. Nevertheless, in view of the potential applications there is an intense search for the ideal magnetoelectric single-phase multiferroic [61–69].

Currently there are at least two multiferroic single-phase materials under intense investigation for use in electrically controlled EB applications [44, 45]. Both YMnO_3 and BiFeO_3 order antiferromagnetically with Néel temperatures of 90 and

643 K, respectively. Despite their AF order the terminology multiferroics is still applied in the literature in a somewhat generalized sense.

Complete electrically induced suppression of EB has been achieved at $T=2$ K in an YMnO_3/Py heterostructure when applying a voltage of 1.2 V across the c-axis of the hexagonal YMnO_3 film of 90 nm thickness [44]. So far, the effect is, however, irreversible which means that a voltage of opposite sign does not recover any EB effect. Moreover, the limitation to low temperatures makes it an interesting system for proof of principle but little attractive for the envisioned applications.

This situation changes in part when BiFeO_3 is used as an electrically controllable pinning layer [45]. In heterostructures of the type $\text{BiFeO}_3/\text{CoFe}$ 10 times higher electric potential differences of ± 12 V were applied across the 100–150 nm thick BiFeO_3 films. The resulting electric fields achieved local magnetization reversal on a lateral length scale of about 2 μm . The limitation to local switching seems to originate from the characteristic domain pattern of the AF, ferroelectric, and ferroelastic order parameters. It remains to be shown if this limitation can be overcome. Subsequently, it is shown that magnetoelastic coupling alone is a very effective and simple way to achieve electrically controlled magnetization.

6.2.3 Piezomagnetically and Piezoelectrically Tuned Exchange Bias

As discussed above, one of the major challenges which microscopic theories of EB face is to explain the quantitative presence of net AF interface magnetization remaining stationary during the FM reversal. The details of the frozen interface magnetization in various systems are affected by a huge variety of crucial influences. Very likely this is one of the reasons why “the origin of EB” has not yet been found in terms of a universal mechanism despite countless attempts. It seems more likely that there is nothing like the universal microscopic mechanism. Many microscopic processes can lead to AF interface magnetization which couples with the adjacent ferromagnet giving rise to EB. For this reason even today a phenomenological description of the EB effect like the Meiklejohn–Bean approach is still valuable.

An exotic possible origin or at least contribution to EB is found for instance in the rutile structured antiferromagnet FeF_2 . The latter has been extensively studied as a prototypical EB pinning system. Compensated and uncompensated AF surfaces can be realized via (111) or (100) surfaces. The (111) surface has been studied at length in order to understand the origin of AF interface magnetization in the particularly puzzling case of compensated surfaces. In addition to the impact of surface roughness and defects which may create random field-type AF domains [70, 71] a more exotic mechanism of stress-induced piezomagnetism has been discussed as one of the possible contributions to the AF interface magnetization [72–75].

Piezomagnetism is known to create the vertical shift of the EB hysteresis loops in $\text{FeF}_2(110)/\text{Fe}$ [76]. Since correlation between the horizontal and vertical loop

shifts is well known [77] it is straightforward to correlate piezomagnetism also with EB fields. The concept of an activation of the symmetry-allowed piezomagnetism in FeF_2 via lattice mismatch-induced stress has been more systematically evidenced in an investigation of the EB heterostructure $\text{Fe}_{0.6}\text{Zn}_{0.4}\text{F}_2/\text{Fe}$. Here external shear stress along the [110] direction activates a piezomoment within the (110) plane that contributes to the AF interface magnetization S_{AF} and, hence, to the EB field [78].

More generally, stress-induced control of magnetic anisotropy which potentially includes also unidirectional anisotropy is a very promising tool to achieve electric control over magnetic states in very simple heterostructures. The use of magnetoelastic coupling for electrically controlled magnetism is well known from investigations of two-phase multiferroics which include artificially grown ferroelectric/ferromagnetic heterostructures such as $\text{BaTiO}_3/\text{La}_{0.66}\text{Sr}_{0.33}\text{MnO}_3$, $\text{BiFeO}_3/\text{SrTiO}_3$, nanopillar-embedded structures of $\text{BaTiO}_3-\text{CoFe}_2\text{O}_4$ or $\text{BiFeO}_3-\text{CoFe}_2\text{O}_4$, $\text{Pb}(\text{Zr}, \text{Ti})\text{O}_3/\text{CoPd}$, and $\text{Pb}(\text{Zr}, \text{Ti})\text{O}_3/\text{terfenol-D}$ [79–84]. The magnetoelastic behavior of these composite materials resembles the product properties of the magnetoelastic effect of the ferromagnetic component and the piezoelectric effect of the (relaxor) ferroelectric [85]. Complex oxides have been some of the most favored materials.

Recently, however, reversible control of magnetism has been reported for a remarkably simple ferroelectric/FM heterostructure. A polycrystalline Fe thin film deposited on the c-plane of a BaTiO_3 single crystal shows a large magnetization change in response to the ferroelectric switching and structural transitions of BaTiO_3 controlled by applied electric fields and temperature, respectively [86]. Interface strain coupling is the primary mechanism altering the induced magnetic anisotropy. As a result, coercivity changes up to 120% occur between the various structural states of BaTiO_3 . Up to 20% coercivity change has been achieved via electrical control at room temperature. This is remarkable considering the fact that the change of the BaTiO_3 lattice parameter within the c-plane is only a secondary effect of the far more pronounced piezoelectric deformation of the c-axis when the electric field is applied along the latter in the tetragonal phase of BaTiO_3 . Hence, much larger effects can still be expected. The concept of ferro- or piezoelectrically controlled magnetism can be straightforward generalized toward electrically controlled EB when taking advantage of the fact that the magnetoelastic coupling constant of some antiferromagnets like CoO is even higher than the corresponding values for the simple 3d metals [87].

6.3 Magnetic Field Control of Exchange Bias

The easiest way to tune the EB field in common EB heterostructures is achieved via the initializing field-cooling process. It takes place in the presence of a freezing field, h_f , applied on cooling the heterostructure to below the Néel temperature, T_N , of the AF pinning layer. Here, the orientation of the freezing field can select either negative or positive EB fields [69]. Note, however, that the positive EB fields established in

$h_f < 0$ have nothing in common with the effect known as positive EB. The latter is observed only when positive (negative) freezing fields give rise to positive (negative) EB fields. Positive EB is a rather unusual case but sometimes observed in systems where the interface exchange interaction is AF and, at the same time, the freezing field applied during the field-cooling procedure is strong enough to overcome the exchange interaction on cooling the system to below the blocking temperature [88–90].

Figure 6.4 illustrates this situation and clarifies a common misconception which confuses the presence of positive EB fields with a sufficient condition to identify the positive EB effect. The Zeeman energy of the interface magnetization in a freezing field favors parallel alignment of S_{AF} with respect to S_{FM} . AF interface coupling in turn favors antiparallel alignment of S_{AF} with respect to S_{FM} . The net effects of the competition between these two energies on the EB field has been experimentally and theoretically studied for instance in Ref. [91]. Inspection of Fig. 6.4 illustrates intuitively that the measurement of the EB field in a single freezing field is not an appropriate tool to determine the sign of the interface coupling, J . In fact, independent of the sign of J , field cooling allows setting the EB field at negative and positive values [92]. Next these details and the specific case of positive EB are discussed with the help of the spin structures displayed in Fig. 6.4.

The two upper frames of Fig. 6.4 show sketches of hysteresis loops after field cooling an EB heterostructure with FM interface coupling $J > 0$ in positive (left upper frame) and negative (right upper frame) freezing fields h_f . When applying h_f at $T > T_N$ no AF long-range order has established and pinning is absent. Hence, the FM top layer is free to align parallel to h_f giving rise to $S_{FM} > 0$ in $h_f > 0$ and $S_{FM} < 0$ in $h_f < 0$. This state of S_{FM} affects the orientation of the AF interface magnetization which establishes on cooling to below T_N . The coupling energy $J S_{AF} S_{FM}$ together with the Zeeman energy control the orientation of S_{AF} . In the case $J > 0$ both the exchange interaction and the Zeeman energy favor parallel alignment of S_{AF} and S_{FM} such that $J S_{AF} > 0$ for $h_f > 0$ and $J S_{AF} < 0$ for $h_f < 0$. Since S_{FM} follows the overall magnetization of the FM layer during a hysteresis loop it is the sign of the stationary product $J S_{AF}$ that determines the sign of the EB field in accordance with Eq. (6.1). Hence, in the case of $J > 0$ negative (positive) EB fields are achieved in positive (negative) freezing fields. Obviously, the positive EB field shown in the upper right frame has nothing in common with the phenomenon of positive EB.

The more complex scenario appears in the case of AF exchange coupling $J < 0$. Both of the two lower frames of Fig. 6.4 show sketches of hysteresis loops after field cooling an EB heterostructure with AF interface coupling in positive freezing fields. The lower left frame displays the situation of field cooling in a moderate magnetic field $0 < h_f < |J S_{FM}|$. Again, when applying h_f at $T > T_N$ there is no pinning effect and the FM top layer aligns parallel to $h_f > 0$ giving rise to $S_{FM} > 0$. The coupling energy $J S_{AF} S_{FM}$ favors now antiparallel alignment of S_{AF} relative to $S_{FM} > 0$. The product $J S_{AF} < 0$ can be interpreted as an exchange field acting on the AF interface magnetization S_{AF} on cooling. At the same time, S_{AF} has potential or Zeeman energy in the applied freezing field $h_f > 0$ which favors $S_{AF} > 0$.

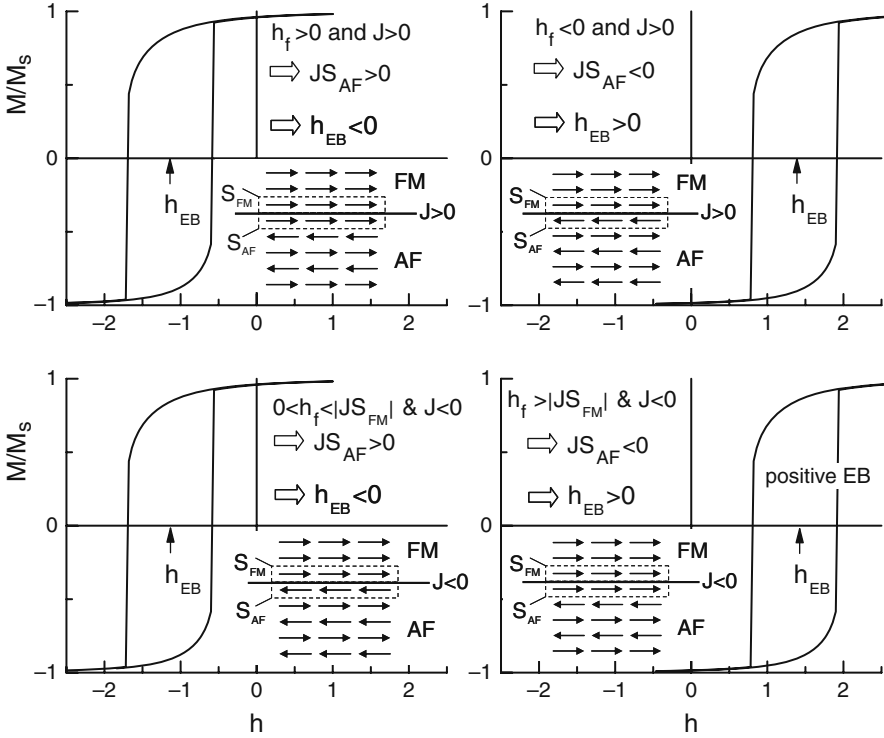


Fig. 6.4 Hysteresis loops of an ideal EB heterosystem with FM interface coupling $J > 0$ (upper left and right frames) and AF interface coupling $J < 0$ (lower left and right frames). For $J > 0$ (upper frames) negative (positive) EB fields h_{EB} are indicated by arrows and achieved by field cooling in a freezing field $h_f > 0$ ($h_f < 0$). For $J < 0$ (upper frames) field cooling in $0 < h_f < |JS_{FM}|$ creates a regular negative EB field while field cooling in $h_f > |JS_{FM}|$ gives rise to a positive EB field which is the fingerprint of the positive EB effect. The frozen AF spin structure and the FM spin structure during the field-cooling process are depicted by arrows. The ideal interface is indicated by a solid line, AF and FM interface spins are marked by boxes (dashed lines).

However, as long as $0 < h_f < |JS_{FM}|$ is fulfilled, the interface exchange energy overcomes the Zeeman energy resulting in $S_{AF} < 0$ and, hence, $JS_{AF} > 0$ giving rise to a regular negative EB field despite $J < 0$.

The situation changes, however, in the case of large positive freezing fields $h_f > |JS_{FM}|$. Now the Zeeman energy overcomes the AF interface coupling giving rise to a parallel alignment of S_{AF} and S_{FM} during the field-cooling process. Hence, $JS_{AF} < 0$ results in a positive EB field in accordance with Eq. (6.1). The latter scenario displayed in the lower right frame of Fig. 6.4 describes the positive EB effect. Out of all situations displayed in Fig. 6.4, only here a positive freezing field gives rise to a positive EB field due to AF interface coupling. Of course one can

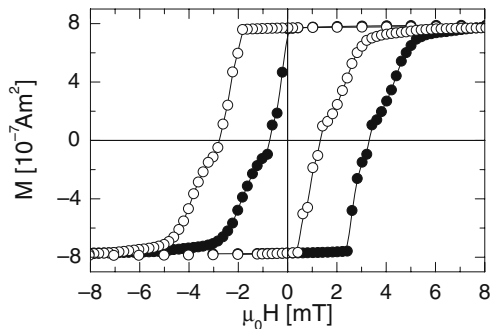
repeat the arguments above for the analogous situation of negative EB fields when field cooling took place in negative freezing fields.

Tuning the EB field by cooling heterostructures in the presence of an applied magnetic field to below the blocking temperature is experimentally straightforward to do but not very attractive for most applications. Here, temperature is typically not a control parameter and the EB field needs to be tuned just with the applied magnetic field at about room temperature. For an AF system an applied homogeneous magnetic field affects the AF long-range order in many ways similarly as temperature does. Increased temperature and increased magnetic fields weaken or even completely suppress AF long-range order. It is therefore not surprising that even below T_B strong magnetic fields typically of the order of several 10 T can set the EB field to a new value which is observed when FM hysteresis loops are measured in moderate magnetic fields significantly smaller than the set field [93]. Again, for applications, it is far more attractive to achieve such a resetting of the EB with set fields of the order of 1 T or below such that no high-field technology is needed.

Recently, Cr_2O_3 has been used as an AF pinning system in a magnetic trilayer structure having two $\text{Cr}_2\text{O}_3/\text{Fe}$ EB interfaces [94]. Here, similar to the magneto-electrically switchable interface magnetization in $\text{Cr}_2\text{O}_3(111)/\text{CoPt}$ the AF surface magnetization in $\text{Cr}_2\text{O}_3(111)/\text{Fe}$ can be isothermally tuned by moderate applied magnetic fields.

Figure 6.5 shows two room temperature hysteresis loops of an Fe 10 nm/ Cr_2O_3 2.72 nm/Fe 10.8 nm trilayer structure after subjecting the system to negative (open circles) and positive (solid circles) DC fields of 1 T magnitude, respectively. The sign of the EB field is controlled exclusively by the applied set field. This is reminiscent of the scenario of changing the sign of the EB field depending on the strength of the cooling fields [86]. Note, however, that here EB tuning takes place isothermally. The pinning magnetization is reversed by a magnetic field only without breaking and reestablishing AF long-range order during a field-cooling process. Competition between AF exchange coupling of the pinning and the Fe magnetizations with the Zeeman interaction energy of the pinning system determines the sign of the EB field. For set fields $\mu_0 H_{DC} \leq 0.2\text{T}$, AF coupling remains dominant

Fig. 6.5 Room temperature hysteresis loops of Fe10nm/ Cr_2O_3 2.72 nm Fe 10.8 nm trilayer after subjecting the system isothermally to $\mu_0 H_{DC} = -1\text{T}$ (open circles) and $\mu_0 H_{DC} = 1\text{T}$ (solid circles) DC magnetic fields. Lines are guide to the eye



over the Zeeman energy, resulting in regular (negative) EB. For larger $\mu_0 H_{DC}$, the Zeeman interaction overcomes the AF exchange coupling which aligns the pinning moments parallel to larger $\mu_0 H_{DC}$, leading to positive EB. The fact that very moderate magnetic fields are sufficient to isothermally tune the EB fields at room temperature promises applicability of this interesting effect in future spintronic devices.

So far we considered various possibilities in tuning the EB field by electric, thermal, and/or magnetic means. It has been mentioned earlier in this chapter that the EB fields can change with consecutively cycled hysteresis loops. Subsequently more light is shed on the physics of the training effect and means to tune strength and other characteristics of the training effect are presented.

6.4 Training Effect in Exchange-Coupled Bilayers

6.4.1 Physical Background of Training Effects in Various Systems

In a general sense training at finite temperature is observed as a consequence of changes in the spin structure taking place in most cases¹ away from a nonequilibrium toward an equilibrium configuration. This training effect deviates from the well-known aging phenomena in magnetic systems [95–100] by the fact that the spin configurational changes in the pinning system are triggered by the magnetic hysteresis loop of the pinned magnetic component which is magnetically coupled with the pinning system. The latter is AF in regular EB systems but can be a spin glass or a hard ferromagnet with a coercivity significantly larger than the coercivity of the pinned system.

Figure 6.6 shows a comparison of the physical mechanism of the training effect in regular AF/FM EB systems and hard/soft all FM bilayers. In both cases there is a pinning and a pinned layer. It is the pinning layer that experiences spin configurational changes on successively cycling the pinned layer through its magnetic hysteresis loop. The left column of sketches displays a regular AF/FM EB system where the pinning layer is an antiferromagnet. The right column displays an all FM hard/soft bilayer system. Here the pinning layer is a hard ferromagnet (HL). A soft ferromagnetic layer (SL) is pinned via AF RKKY interaction to the HL. In both cases the pinning layer can be initialized into a domain state which deviates from its perfect long-range order. In the case of an AF pinning layer an AF domain state is created during the field-cooling procedure which, in compensated EB systems, induces magnetization in the AF pinning layer and with that AF interface magnetization S_{AF} giving rise to EB in accordance with Eq. (6.1). Subsequently cycled hysteresis loops trigger spin configurational changes in the pinning layer which

¹ Hoffmann discussed the zero temperature training effect in EB systems with multiple AF easy anisotropy axes in terms of a triggered transition driving the pinning layer away from the equilibrium [31].

drive the antiferromagnet closer toward perfect long-range order characterized by the equilibrium AF order parameter η_e . The latter approach toward a new quasi-equilibrium spin configuration is accompanied by a decay of S_{AF} with increasing number of loops, n . The degrading AF interface magnetization reduces the magnitude of the EB field. This process resembles the training effect. It is again in accordance with Eq. (6.1) when a static interface magnetization is generalized into $S_{AF} = S_{AF}(n)$.

An analogous scenario takes place in the exchange-coupled HL/SL bilayers [3]. Here the initialization of the out-of-equilibrium domain state of the pinning layer is isothermally achieved by applying a negative (positive) set field after positive (negative) saturation of the HL. The sketches in the right column of Fig. 6.6 illustrate the HL domain state after its initializing in a negative set field (top). In this state the overall magnetization of the HL is reduced with respect to its saturation value and with it the HL interface magnetization. Therefore, the HL/SL coupling energy is reduced when the HL is in a FM domain state and the bias field characterizing the

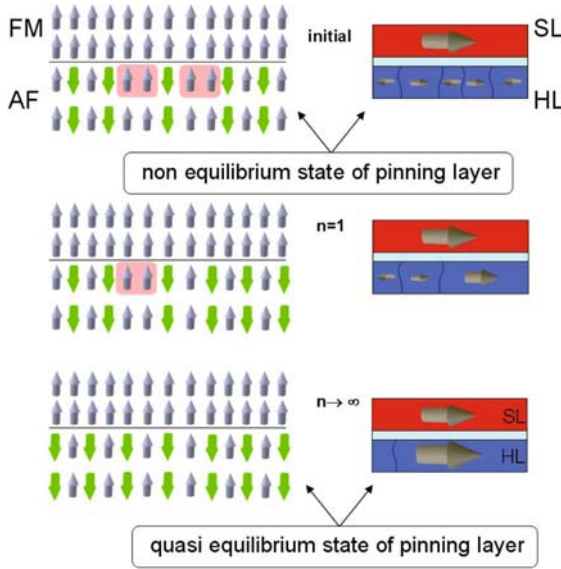


Fig. 6.6 Comparison of the training effect in an AF/FM and a HL/SL heterostructure. The left column depicts three sketches of an AF/FM EB heterostructure after initializing EB (top), after the first (middle), and after a very large number of hysteresis loops (bottom). The nonequilibrium AF domain state carries magnetization to the interface (horizontal line). Neighboring spin pairs with non-compensating moment contributing to S_{AF} are highlighted. The quasi-equilibrium state reflects the asymptotic approach of nearly perfect AF long-range order. S_{AF} is reduced and so is the EB field. The right column depicts sketches of a HL/SL heterostructure after initializing a FM domain state (top), after the first SL hysteresis loop (middle), and after a very large number of hysteresis loops (bottom). The nonequilibrium cycling when the domain state asymptotically approaches nearly perfect FM long-range order

loop shift of the SL hysteresis is low. Subsequent SL hysteresis loops trigger spin configurational changes in the HL. The latter approaches asymptotically a quasi-equilibrium state of increased magnetization M_e . The increase in HL magnetization gives rise to an increase in its interface magnetization which increases the bias field.

Figure 6.7 displays the evolution of the free energy ΔF of the AF (upper left) and the FM HL (upper right) pinning layer when they change from their respective nonequilibrium states with order parameters η and M into the quasi-equilibrium states η_e and M_e . The pinning layer domain states associated with η and M and the final states associated with η_e and M_e are sketched, respectively. A harmonic approximation (dashed parabolas) of the Landau free energy landscape of the double well type catches already the essentials necessary to describe the triggered relaxation toward equilibrium quantitatively. The left bottom frame of Fig. 6.7 shows the evolution, $\mu_0 H_{EB}$ vs. n , of the EB field of the $\text{Cr}_2\text{O}_3/\text{Fe}$ heterostructure introduced previously. The solid squares are experimental data obtained from the hysteresis loop shifts measured at $T=300$ K by SQUID magnetometry. Open circles connected with eye-guiding lines are results of a single parameter fit of Eq. (6.5). The inset shows the 1st (solid diamonds), the 2nd (open diamonds), and the 10th (stars) hysteresis loop. The right bottom frame of Fig. 6.7 displays the evolution, $\mu_0 H_B$ vs. n , of the bias field of the all FM HL/SL system CoPtCrB 15 nm (HL)/ Ru 0.7 nm/ CoCr 3 nm (SL) [3]. The solid squares are experimental data obtained from the SL hysteresis loop shifts measured at $T=395$ K by SQUID magnetometry. The line represents a single parameter best fit of Eq. (6.4). Note that only integer values of n have physical meaning. The inset shows the 1st (solid diamonds), 2nd (open diamonds), and the 15th (stars) hysteresis loop of the SL. Despite the intuitive similarities between these two training phenomena the details of the EB and bias field evolution show significant differences in particular for the transition $n=1$ to $n=2$ but also for the asymptotic behavior.

Next we briefly sketch how these differences are reflected in the theoretical description. The latter has been introduced in Ref. [26] and is based on a discretized form of the Landau–Khalatnikov equation² which reads [26, 3]

$$\frac{S_{\text{AF/HL}}(n+1) - S_{\text{AF/HL}}(n)}{\tau} = -\frac{1}{\xi} \frac{\partial \Delta F}{\partial S_{\text{AF/HL}}} \quad (6.3)$$

for AF or ferromagnetic HL pinning systems, respectively. Figure 6.7 shows the harmonic approximation in the vicinity of the equilibrium used to obtain the simplest expressions for the free energy entering Eq. (6.2). In the case of all FM HL/SL systems the order parameter M is proportional to the interface magnetization S_{HL} which leads with the help of Eq. (6.3) straightforward to the explicit expression [3]

² While details of the dynamics between states n and $n+1$ are not relevant, the use of the discretized Landau Khalatnikov dynamic equation has to be justified. It is appropriate since the integral magnetization of the pinning layer is non-conserved.

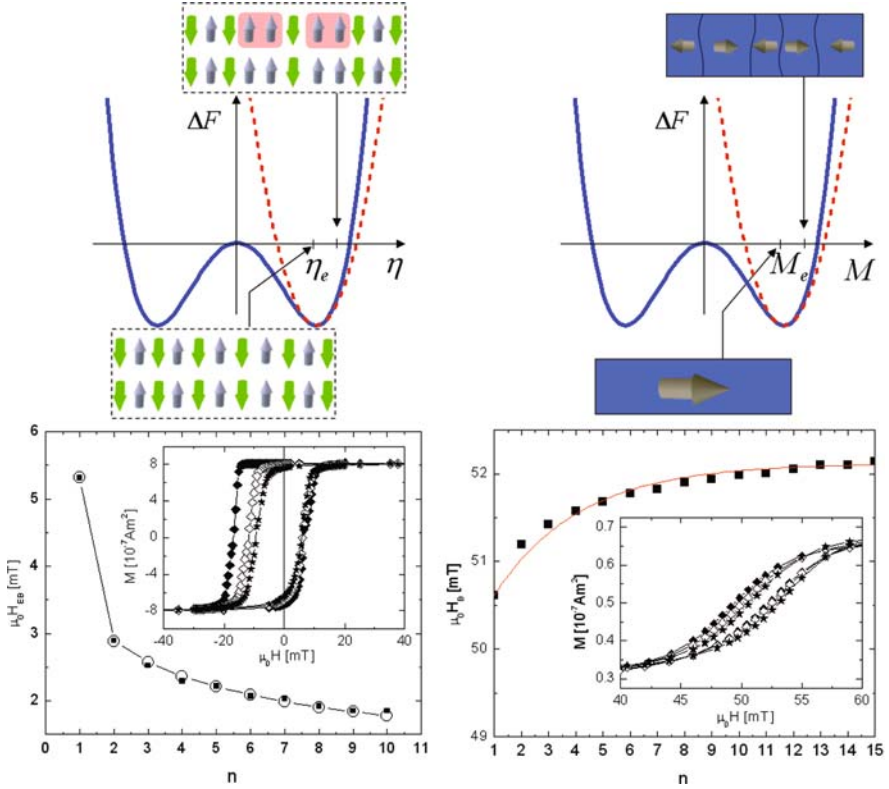


Fig. 6.7 Free energy ΔF vs. η (upper left graph) and M (upper right graph) for AF and FM pinning systems, respectively. Arrows assign sketches of the spin and domain structures of AF and FM (non)equilibrium states (η and M) η_e and M_e to the free energy graphs. Dashed lines show harmonic approximations of the Landau free energy landscape. The bottom left frame shows $\mu_0 H_{EB}$ vs. n for $\text{Cr}_2\text{O}_3/\text{Fe}$. The solid squares are experimental data measured at $T=300$ K. Open circles connected with eye-guiding lines are results of a single parameter fit of Eq. (6.4). The inset shows the 1st (solid diamonds), 2nd (open diamonds), and the 10th (stars) hysteresis loop. The bottom right frame displays $\mu_0 H_B$ vs. n of $\text{CoPtCrB } 15 \text{ nm/Ru } 0.7 \text{ nm/CoCr } 3 \text{ nm}$. Solid squares are experimental data measured at $T=395$ K. The line represents a single parameter best fit of Eq. (6.3). The inset shows the 1st (solid diamonds), 2nd (open diamonds), and 15th (stars) hysteresis loop of the SL.

$$\mu_0 H_B(n) = (K+1)^{n-1} \left\{ \mu_0 H_B(n=1) - K \mu_0 H_B^c \left[\frac{(K+1)^{n+1} - 1}{K(K+1)^{n-1}} - (K+2) \right] \right\}, \quad (6.4)$$

where $0 < K < 1$ is the fitting parameter that determines the rate of change of the bias field approaching the equilibrium value $\mu_0 H_B^c$ with exponential asymptotic.

The relation between the AF order parameter η and the interface magnetization S_{AF} is somewhat more involved [27]. With the help of the corresponding free energy expression one obtains the implicit sequence [26,27,29]

$$\mu_0(H_{\text{EB}}(n+1) - H_{\text{EB}}(n)) = -\gamma(\mu_0(H_{\text{EB}}(n) - H_{\text{EB}}^{\text{e}}))^3, \quad (6.5)$$

where the fitting parameter γ controls the rate of change of the EB field approaching the equilibrium EB field $\mu_0 H_{\text{EB}}^{\text{e}}$ with a $1/\sqrt{n}$ asymptotic behavior. The latter has been successfully applied very early as an empirical expression first suggested in Ref. [21]. Its consistency with the asymptotic behavior of Eq. (6.5) is a strong confirmation of the theoretical approach sketched here.

6.4.2 Tuning the Training Effect

From the previous discussion it can be concluded that any means affecting the initial spin structure of the pinning layer will have an impact on the training behavior. Therefore, one has to expect that training characteristics can be tuned with the help of magnetic fields strong enough to perturb the AF pinning layer. Recently it has been shown in NiO/Ni bilayers that a training behavior following Eq. (6.5) can be perturbed by a large out-of-plane magnetic field of about 1 T such that subsequent training data show a substantially accelerated training effect [101]. Brems et al. showed that it is possible in CoO/Co bilayers to partially reinduce the untrained state when measuring a hysteresis loop with an in-plane external field perpendicular to the cooling field [102]. A simultaneous isothermal quenching of training and EB has been achieved in the Fe/Cr₂O₃/Fe trilayer introduced above. After field cooling from $T=395$ K in $\mu_0 H = 50$ mT down to $T = 20$ K the system shows a large EB and EB training effect. However, when subjecting the system to large in-plane DC magnetic field of 7 T EB bias and with it EB training is completely quenched [103].

The AF order parameter of the pinning systems in regular AF/FM EB heterostructures does not directly couple to homogeneous applied magnetic fields. Therefore, all of the effects described above require either large fields or sources for significant imbalance in the sublattice magnetizations such as thermal excitation or imperfections giving rise to deviation from perfect AF long-range order. In all FM heterostructures the situation is different. Here, homogeneous applied magnetic fields are conjugate to the FM order parameter of the pinning system and can directly influence the magnetic state of the latter. A systematic field-induced variation of the training behavior has been demonstrated and the characteristics of the training effect have been directly related to the field-controlled magnetization of the pinning layer [3].

Equation (6.3) shows that training is a triggered relaxation phenomenon. Hence one has to expect that the magnetic sweep rate of the hysteresis loops also affects the relaxation dynamics of the pinning system. In accordance with this intuitive qualitative picture a dynamic enhancement of the exchange bias training effect has been observed in the same all FM bilayer discussed above [28]. A similar enhancement has been observed in regular AF/FM heterostructures as well [26].

6.5 Conclusion

This chapter reviewed selected modern attempts to tune the characteristics of a number of effects associated with the exchange bias phenomenon. The most prominent is certainly the emergence of an exchange bias field in field-cooled antiferromagnetic/ferromagnetic thin film heterostructures. Control of the exchange bias field has been reviewed with special emphasis on electrically controlled exchange bias. Its successful integration in novel device architectures promises tremendous impact on future spintronic applications. The exchange bias training effect is a less investigated field with many open questions on a microscopic level. A simple but powerful phenomenological description of the training effect has been introduced and its universality has been evidenced. In accordance with this intuitive understanding various attempts to control the exchange bias and its training effect have been reported.

Acknowledgments This chapter is supported in part by NSF through Career DMR-0547887, MRSEC DMR-0213808, NCMN, and NRI. The author gratefully acknowledges discussions with Sarbeswar Sahoo, Srinivas Polisetty, Xi He, Yi Wang, and Tathagata Mukherjee.

References

1. Th. Mühge, N. N. Garif'yanov, Yu. V. Goryunov, G. G. Khaliullin, L. R. Tagirov, K. Westerholt, I. A. Garifullin, and H. Zabel, "Possible Origin for Oscillatory Superconducting Transition Temperature in Superconductor/Ferromagnet Multilayers" *Phys. Rev. Lett.* **77**, 1857 (1996).
2. Chun-Gang Duan, S. S. Jaswal, and E. Y. Tsymbal, "Predicted Magnetoelectric Effect in Fe/BaTiO₃ Multilayers: Ferroelectric Control of Magnetism" *Phys. Rev. Lett.* **97**, 047201 (2006).
3. Ch. Binek, S. Polisetty, Xi He, and A. Berger, "Exchange Bias Training Effect in Coupled All Ferromagnetic Bilayer Structures" *Phys. Rev. Lett.* **96**, 067201 (2006).
4. I. Žutić, J. Fabian, and S. Das Sarma, "Spintronics: Fundamentals and applications" *Rev. Mod. Phys.* **76**, 323 (2004).
5. G. E. Moore, "Cramming more components onto integrated circuits" *Electronics* **38**, 114 (1965).
6. W. H. Meiklejohn and C. P. Bean, "New Magnetic Anisotropy" *Phys. Rev.* **102**, 1413 (1956).
7. W. H. Meiklejohn and C. P. Bean, "New Magnetic Anisotropy" *Phys. Rev.* **105**, 904 (1957).
8. J. Nogués and I.K. Schuller, "Exchange bias" *J. Magn. Magn. Mater.* **192**, 203 (1999).
9. A. Berkowitz and K. Takano, "Exchange anisotropy- a review" *J. Magn. Magn. Mater.* **200**, 552 (1999).
10. R. L. Stamps, "Mechanisms for exchange bias", *J. Phys. D* **33**, R247 (2000).
11. M. Kiwi, "Exchange bias theory", *J. Magn. Magn. Mater.* **234**, 584 (2001).
12. M. Ali, P. Adie, C. H. Marrows, D. Greig, B. J. Hickey, and R. L. Stamps, "Exchange bias using a spin glass" *Nat. Mater.* **6**, 70 (2007).
13. I. Roshchin, O. Petravic, R. Morales, Z.-P. Li, X. Battle, and I. K. Schuller, "Lateral length scales in exchange bias" *Europhys. Lett.* **71**, 297 (2005).
14. F. Radu and H. Zabel, "Exchange bias effect of ferro-/antiferromagnetic heterostructures" *Springer Tracts Modern Phys.*, **227** (2008).
15. W. Kuch, L. I. Chelaru, F. Offi, J. Wang, M. Kotsugi, and J. Kirschner, "Tuning the magnetic coupling across ultrathin antiferromagnetic films by controlling atomic-scale roughness" *Nat. Mater.* **5**, 128 (2006).
16. J. S. Jiang, G. P. Felcher, A. Inomata, R. Goyette, C. S. Nelson, and S. D. Bader, "Exchange bias in Fe/Cr double superlattices" *J. Vac. Sci Technol. A* **18**, 1264 (2000).

17. F. Nolting, A. Scholl, J. Stöhr, J. W. Seo, J. Fompeyrine, H. Siegwart, J.-P. Locquet, S. Anders, J. Lüüing, E. E. Fullerton, M. F. Toney, M. R. Scheinfein, and H. A. Padmore, “*Direct observation of the alignment of ferromagnetic spins by antiferromagnetic spins*” *Nature* **405**, 767 (2000).
18. Ch. Binek, A. Hochstrat, and W. Kleemann, “*Exchange Bias in a generalized Meiklejohn-Bean approach*” *J. Magn. Magn. Mater.* **234**, 353 (2001).
19. C. Leighton, J. Nogués, B. J. Jönsson-kerman, and I.K. Schuller, “*Coercivity Enhancement in Exchange Biased Systems Driven by Interfacial Magnetic Frustration*” *Phys. Rev. Lett* **84**, 3466 (2000).
20. S. Maat, K. Takano, S. S. P. Parkin, and E. E. Fullerton, “*Perpendicular Exchange Bias of Co/Pt Multilayers*” *Phys. Rev. Lett* **87**, 087202 (2001).
21. G. Scholten, K. D. Usadel, and U. Nowak, “*Coercivity and exchange bias of ferromagnetic/antiferromagnetic multilayers*” *Phys. Rev. B* **71**, 064413 (2005).
22. D. Paccard, C. Schlenker, O. Massenet, R. Montmory, and A. Yelon, “*A New Property of Ferromagnetic-Antiferromagnetic Coupling*” *Phys. Status Solidi* **16**, 301 (1966).
23. C. Schlenker, S. S. P. Parkin, J. C. Scott, and K. Howard, “*Magnetic disorder in the exchange bias bilayered FeNi-FeMn system*” *J. Magn. Magn. Mater.* **54**, 801 (1986).
24. K. Zhang, T. Zhao, and M. Fujiwara, “*Training effect of exchange biased iron-oxide/ferromagnet systems*”, *J. Appl. Phys.* **89**, 6910 (2001).
25. S. G. te Velthuis, A. Berger, G. P. Felcher, B. Hill, and E. Dahlberg, *J. Appl. Phys.* **87**, 5046 (2000).
26. Heiwan Xi, R. M. White, S. Mao, Z. Gao, Z. Yang, and E. Murdock, “*Low-frequency dynamic hysteresis in exchange-coupled Ni₈₁Fe₁₉/Ir₂₂Mn₇₈ bilayers*” *Phys. Rev. B* **64**, 184416 (2001).
27. Ch. Binek, “*Training of the exchange-bias effect: A simple analytic approach*” *Phys. Rev. B* **70**, 014421 (2004).
28. Ch. Binek, Xi He and S. Polisetty, “*Temperature dependence of the training effect in a Co/CoO exchange-bias layer*” *Phys. Rev. B* **72**, 054408 (2005).
29. S. Sahoo, S. Polisetty, Ch. Binek, and A. Berger, ” *Dynamic enhancement of the exchange bias training effect*” *J. Appl. Phys.* **101**, 053902 (2007).
30. S. Polisetty, S. Sahoo, and Ch. Binek, “*Scaling Behavior of the Exchange-Bias Training Effect*” *Phys. Rev. B.* **76**, 184423 (2007).
31. Haiwen Xi, S. Franzen, S. Mao, and R. M. White, “*Exchange bias relaxation in reverse magnetic fields*” *Phys. Rev. B* **75**, 014434 (2007).
32. A. Hoffmann, “*Symmetry Driven Irreversibilities at Ferromagnetic-Antiferromagnetic Interfaces*” *Phys. Rev. Lett.* **93**, 097203 (2004).
33. V. Skumryev, S. Stoyanov, Y. Zhang, G. Hadjipanayis, D. Givord, and J. Nogués, “*Beating the superparamagnetic limit with exchange bias*” *Nature (London)* **423**, 850 (2003).
34. A. Hochstrat, Ch. Binek, and W. Kleemann, “*Training of the exchange-bias effect in NiO-Fe heterostructures*” *Phys. Rev. B* **66**, 092409 (2002).
35. Yan-kun Tang, Young Sun, and Zhao-hua Cheng, “*Exchange bias associated with phase separation in the perovskite cobaltite La_{1-x}Sr_xCoO₃*” *Phys. Rev. B* **73**, 174419 (2006).
36. D. Niebieskikwiat, and M. B. Salamon, “*Intrinsic interface exchange coupling of ferromagnetic nanodomains in a charge ordered manganite*” *Phys. Rev. B* **72**, 174422 (2005).
37. R. Ang, Y. P. Sun, X. Luo, C. Y. Hao, X. B. Zhu, and W. H. Song, “*The evidence of the glassy behavior in the layered cobaltites*” *Appl. Phys. Lett.* **92**, 162508 (2008).
38. S. Karmakar, S. Taran, E. Bose, and B. K. Chaudhuri, C. P. Sun, C. L. Huang, and H. D. Yang, “*Evidence of intrinsic exchange bias and its origin in spin-glass-like disordered L_{0.5}Sr_{0.5}MnO₃ manganites (L=Y, Y_{0.5}Sm_{0.5}, and Y_{0.5}La_{0.5})*” *Phys. Rev. B* **77**, 144409 (2008).
39. J. Ventura, J. P. Araujo, J. B. Sousa, A. Veloso, and P. P. Freitas, “*Training effect in specular spin valves*” *Phys. Rev. B* **77**, 184404 (2008).
40. W. Eerenstein, N. D. Mathur, J. F. Scott, “*Multiferroic and magnetoelectric materials*” *Nature* **442** 759 (2006).

41. N.A. Hill, "Why are there so few magnetic ferroelectrics?" J. Phys. Chem. B **140**, 6694 (2000).
42. P. Borisov, A. Hochstrat, Xi Chen, W. Kleemann, and Ch. Binek, "Magnetoelectric Switching of Exchange Bias" Phys. Rev. Lett. **94**, 117203 (2005).
43. Ch. Binek, P. Borisov, X. Chen, A. Hochstrat, S. Sahoo, and W. Kleemann, "Perpendicular exchange bias and its control by magnetic, stress and electric fields" Eur. Phys. J. B **45**, 197 (2005).
44. A. Hochstrat, Ch. Binek, Xi Chen, W. Kleemann, "Extrinsic control of the exchange bias" J. Magn. Magn. Mater. **272**, 325 (2004).
45. Ch. Binek, B. Doudin, "Magneto-electronics with magnetoelectrics" J. Phys. Condens. Matter **17**, L39 (2005).
46. Ch. Binek, A. Hochstrat, X. Chen, P. Borisov, W. Kleemann, and B. Doudin, "Electrically controlled exchange bias for spintronic applications" J. Appl. Phys. **97**, 10C514 (2005).
47. P. Curie, J. de Physique, "Sur la symétrie dans les phénomènes physiques, symétrie d'un champ électrique et d'un champ magnétique" **3**, 393 (1894).
48. I. E. Dzyaloshinskii, "On the magneto-electric effect in antiferromagnets" Sov. Phys. JETP **10** 628 (1960).
49. W. Eerenstein, M. Wiora, J. L. Prieto, J. F. Scott and N. D. Mathur, "Giant sharp and persistent converse magnetoelectric effects in multiferroic epitaxial heterostructures" Nat. Mater. **6**, 348 (2007).
50. S. Alexander and S. Shtrikman, "On the origin of the axial magnetoelectric effect of Cr_2O_3 " Solid State Commun. **4**, 115 (1966).
51. R. Hornreich and S. Shtrikman, "Statistical Mechanics and Origin of the Magnetoelectric Effect in Cr_2O_3 " Phys. Rev. **161**, 506–512 (1967).
52. V. Laukhin, V. Skumryev, X. Martí, D. Hrabovský, F. Sánchez, M.V. García-Cuenca, C. Ferrater, M. Varela, U. Lüders, J. F. Bobo, and J. Fontcuberta, "Electric-Field Control of Exchange Bias in Multiferroic Epitaxial Heterostructures" Phys. Rev. Lett. **97** 227201 (2006).
53. Y.H. Chu, L. W. Martin, M. B. Holcomb, M. Gajek, S. J. Han, Q. HE, N. Balke, C. H. Yang, D. Lee, W. Hu, Q. Zhan, P. L. Yang, A. Fraile-Rodriguez, A. Scholl, S. X. Wang and R. Ramesh, "Electric-field control of local ferromagnetism using a magnetoelectric multiferroic" Nat. Mater. **7**, 478 (2008).
54. P. Borisov, Th. Eimüller, A. Fraile-Rodriguez, A. Hochstrat, X. Chen, W. Kleemann, "Application of the magnetoelectric effect to exchange bias" J. Magn. Magn. Mater. **310**, 2313 (2007).
55. H. Béa, M. Bibes, and S. Cherifi, "Tunnel magnetoresistance and robust room temperature exchange bias with multiferroic $BiFeO_3$ epitaxial thin films" Appl. Phys. Lett. **89**, 242114 (2006).
56. P. Borisov, A. Hochstrat, X. Chen, and W. Kleemann, "Multiferroically composed exchange bias systems" Phase Trans. **79**, 1123 (2006).
57. M. Bibes, and A. Barthélémy "Towards a magnetoelectric memory" Nat. mater. **7**, 425 (2008).
58. S. Sahoo and Ch. Binek, "Piezomagnetism in epitaxial Cr_2O_3 thin films and spintronic applications" Phil. Mag. Lett. **87**, 259 (2007).
59. M. Fiebig, "Revival of the magnetoelectric effect" J. Phys. D: Appl. Phys. **38**, R123 (2005).
60. P. Borisov, A. Hochstrat, V. V. Shvartsman, W. Kleemann, "Superconducting quantum interference device setup for magnetoelectric measurements" Rev. Sci. Instr. **78**, 106105 (2007).
61. T. Kimura, T. Goto, H. Shintani, K. Ishizaka, T. Arima, and Y. Tokura, "Magnetic control of ferroelectric polarization", Nature **426**, 55 (2003).
62. N. Hur, S. Park, P. A. Sharma, J. S. Ahn, S. Guha, and S-W. Cheong, "Electric polarization reversal and memory in a multiferroic material induced by magnetic fields" Nature **429**, 392 (2004).

63. M. Gajek, M. Bibes, S. Fusil, K. Bouzehouane, J. Fontcubert, A. Barthélémy, and A. Fert, "Tunnel junctions with multiferroic barriers" *Nat. Mater.* **6**, 296 (2007).
64. T. Kimura, S. Kawamoto, I. Yamada, M. Azuma, M. Takano, and Y. Tokura, "Magnetocapacitance effect in multiferroic BiMnO_3 " *Phys. Rev. B* **67** 180401(R) (2003).
65. T. Lottermoser, T. Lonkai, U. Amann, D. Hohlwein, J. Ihringer, and M. Fiebig, "Magnetic phase control by an electric field" *Nature* **430**, 541 (2004).
66. J. Hemberger, P. Lunkenheimer, R. Fichtl, H.-A. Krug von Nidda, V. Tsurkan, and A. Loidl, "Relaxor ferroelectricity and colossal magnetocapacitive coupling in ferromagnetic CdCr_2S_4 " *Nature* **434**, 364 (2005).
67. Y. Yamasaki, S. Miyasaka, Y. Kaneko, J. P. He, T. Arima, and Y. Tokura, "Magnetic Reversal of the Ferroelectric Polarization in a Multiferroic Spinel Oxide" *Phys. Rev. Lett.* **96**, 207204 (2006).
68. C. Thiele, K. Dörr, O. Bilani, J. Rödel, and L. Schultz, "Influence of strain on the magnetization and magnetoelectric effect in $\text{La}_{0.7}\text{A}_{0.3}\text{MnO}_3/\text{PMN-PT}(001)$ ($\text{A}=\text{Sr,Ca}$)" *Phys. Rev. B* **75**, 054408 (2007).
69. T. Zhao, A. Scholl, F. Zavaliche, K. Lee, M. Barry, A. Doran, M. P. Cruz, Y. H. Chu, C. Ederer, N. A. Spaldin, R. R. Das, D. M. Kim, S. H. Baek, C. B. Eom, and R. Ramesh, "Electrical control of antiferromagnetic domains in multiferroic BiFeO_3 films at room temperature" *Nat. Mater.* **5**, 823 (2006).
70. A. P. Malozemoff, "Random-field model of exchange anisotropy at rough ferromagnetic-antiferromagnetic interfaces" *Phys. Rev. B* **35**, 3679 (1987).
71. P. Miltényi, M. Gierlings, J. Keller, B. Beschoten, G. Güntherodt, U. Nowak, K. D. Usadel, "Diluted Antiferromagnets in Exchange Bias: Proof of the Domain State Model" *Phys. Rev. Lett.* **84**, 4224 (2000).
72. A. S. Borovik-Romanov, "Piezomagnetism in the antiferromagnetic fluorides of cobalt and manganese" *Sov. Phys. JETP* **11**(1960) 786.
73. I. E. Dzialoshinskii, "The problem of piezomagnetism" *JETP* **33** 807 (1957).
74. J. Kushauer, C. Binek, and W. Kleemann, *J. Appl. Phys.* **75** 5856 (1994).
75. Ch. Binek, "Ising-type antiferromagnets: Model systems in statistical physics and the magnetism of exchange bias" *Springer Tracts Modern Phys.* **196**, (Springer, Berlin, 2003).
76. J. Nogués, T. J. Moran, D. Lederman, I. K. Schuller, and K. V. Rao, "Role of interfacial structure on exchange-biased $\text{FeF}_2\text{-Fe}$ " *Phys. Rev. B* **59**, 6984 (1999).
77. A. Hochstrat, Ch. Binek, and W. Kleemann, "Training of the exchange-bias effect in NiO-Fe heterostructures" *Phys. Rev. B* **66**, 092409 (2002).
78. Ch. Binek, Xi Chen, A. Hochstrat, and W. Kleemann, "Exchange bias in $\text{Fe}_{0.6}\text{Zn}_{0.4}\text{F}_2/\text{Fe}$ heterostructures" *J. Magn. Magn. Mater.* **240**, 257 (2002).
79. M. K. Lee, T. K. Nath, C. B. Eom, M. C. Smoak, and F. Tsui, "Strain modification of epitaxial perovskite oxide thin films using structural transitions of ferroelectric BaTiO_3 substrate" *Appl. Phys. Lett.* **77**, 3547 (2000).
80. X. Qi, H. Kim, and M. G. Blamire, "Exchange bias in bilayers based on the ferroelectric antiferromagnet BiFeO_3 " *Phil. Mag. Lett.* **87**, 175 (2007).
81. J. Wang, J. Neaton, H. Zheng, V. Nagarajan, S. B. Ogale, B. Liu, D. Viehland, V. Vaithyanathan, D. G. Schlom, U. Waghmare, N. A. Spaldin, K. M. Rabe, M. Wuttig, and R. Ramesh, "Epitaxial BiFeO_3 Multiferroic Thin Film Heterostructures" *Science* **299**, 1719 (2003).
82. H. Zheng, J. Wang, S. E. Lofland, Z. Ma, L. Mohaddes-Ardabili, T. Zhao, L. Salamanca-Riba, S. R. Sinde, S. B. Ogale, F. Bai, D. Viehland, Y. Jia, D. G. Schlom, M. Wuttig, A. Roytburd, and R. Ramesh, "Multiferroic $\text{BaTiO}_3\text{-CoFe}_2\text{O}_4$ " Nanostructures *Science* **303**, 661 (2004).
83. F. Zavaliche, H. Zheng, L. Mohaddes-Ardabili, S. Y. Yang, Q. Zhan, P. Shafer, E. Reilly, R. Chopdekar, Y. Jia, P. Wright, D. G. Schlom, Y. Suzuki, and R. Ramesh, "Electric field-induced magnetization switching in epitaxial columnar nanostructures" *Nano Lett.* **5**, 1793 (2005).

84. G. Srinivasan, E. T. Rasmussen, J. Gallegos, R. Srinivasan, Yu. I. Bokhan, and V. M. Laletin, “*Magnetolectric effects in bilayers and multilayers of magnetostrictive and piezoelectric perovskite oxides*” Phys. Rev. B **64**, 214408 (2001).
85. C.W. Nana, “*Magnetolectric effect in composites of piezoelectric and piezomagnetic phases*” Phys. Rev. B **50**, 6082 (1994).
86. S. Sahoo, S. Polisetty, C.-G. Duan, Sitaram S. Jaswal, E. Y. Tsymbal, and Ch. Binek, “*Ferroelectric control of magnetism in BaTiO₃/Fe heterostructures via interface strain coupling*”, Phys. Rev. B **76**, 092108 (2007).
87. B. D. Cullity, *Introduction to magnetic materials*. Reading, MA: Addison-Wesley (1972).
88. J. Nogués, D. Lederman, T. J. Moran, and Ivan K. Schuller, “*Positive Exchange Bias in FeF₂-Fe Bilayers*” Phys. Rev. Lett. **76**, 4624 (1996).
89. J. Nogués, C. Leighton and Ivan K. Schuller, “*Correlation between antiferromagnetic interface coupling and positive exchange bias*” Phys. Rev. B **61**, 1315 (2000).
90. T. L. Kirk, O. Hellwig, and Eric E. Fullerton, “*Coercivity mechanisms in positive exchange-biased Co films and CoPt multilayers*” Phys. Rev. B, **65**, 224426 (2002).
91. B. Kagerer, Ch. Binek, W. Kleemann, “*Freezing field dependence of the exchange bias in uniaxial FeF₂-CoPt heterosystems with perpendicular anisotropy*” J. Magn. Magn. Mater. **217**, 139 (2000).
92. Z. Y. Liu and S. Adenwalla, “*Oscillatory interlayer exchange coupling and its temperature dependence in [Pt/Co]₃/NiO/[Co/Pt]₃ multilayers with perpendicular anisotropy*” Phys. Rev. Lett. **91**, 037207-1 (2003).
93. J. Nogués, J. Sort, S. Suriñach, J. S. Muñoz, M. D. Baró, J. F. Bobo, U. Lüders, E. Haanappel, M. R. Fitzsimmons, A. Hoffmann, and J. W. Cai, “*Isothermal tuning of exchange bias using pulsed fields*” Appl. Phys. Lett. **82**, 3044 (2003).
94. S. Sahoo, T. Mukherjee, K. D. Belashchenko, and Ch. Binek, “*Isothermal low-field tuning of exchange bias in epitaxial Fe/Cr₂O₃/Fe*” Appl. Phys. Lett. **91**, 172506 (2007).
95. T. Jonsson, J. Mattsson, C. Djurberg, F. A. Khan, P. Nordblad, and P. Svedlindh, “*Aging in a Magnetic Particle System*” Phys. Rev. Lett. **75**, 4138 (1995).
96. S. Sahoo, O. Petravic, Ch. Binek, W. Kleemann, J. B. Sousa, S. Cardoso, and P. P. Freitas, “*Magnetic relaxation phenomena in the superspin-glass system [Co₈₀F₂₀/Al₂O₃]₁₀*” J. Phys. Condens. Matter **14**, 6729 (2002).
97. R. Skomski, J. Zhou, R. D. Kirby, and D. J. Sellmyer, “*Magnetic Aging*” Mater. Res. Soc. Symp. Proc. **887**, 133 (2006).
98. M. Pleimling “*Aging phenomena in critical semi-infinite systems*” Phys. Rev. B **70**, 104401 (2004).
99. K. H. Fischer and J. A. Hertz, *Spin Glasses*. Cambridge Univ. Press, Cambridge (1991).
100. J. A. Mydosh, *Spin Glasses: an Experimental Introduction*. Taylor and Francis, London (1993).
101. P. Y. Yang, C. Song, F. Zeng, and F. Pan, “*Tuning the training effect in exchange biased NiO/Ni bilayers*” Appl. Phys. Lett. **92**, 243113 (2008).
102. S. Brems, D. Buntinx, K. Temst, Ch. Van Haesendonck, F. Radu, and H. Zabel, “*Reversing the Training Effect in Exchange Biased CoO/Co Bilayers*” Phys. Rev. Lett. **95**, 157202 (2005).
103. S. Sahoo and Ch. Binek, “*Quenching of the Exchange Bias Training in Fe/Cr₂O₃/Fe Tri-layer*”, AIP. Conf. Proc. **1063**, 132 (2008).